13. H. J. Melosh, *Icarus* **59**, 234 (1984); *Lunar Planet. Sci.* **16**, 548 (1985).
14. V. Ott and F. Begemann, *Nature (London)* **317**, 509 (1985); R. O. Pepin, *The Evolution of the Martian Atmosphere* (Lunar and Planetary Institute, Houston, 1985), pp. 20–21.
15. J. D. O'Keefe and T. J. Ahrens, in *Proceedings of the Eighth Lunar Science Conference* (Pergamon, New York, 1977), p. 3357; *Science* **198**, 1249 (1977).
16. C. Polanskey and T. J. Ahrens, *Lunar Planet. Sci.* **16**, 671 (1985).
17. D. E. Rehfuss, *J. Geophys. Res.* **32**, 6303 (1972).
18. A. V. Singer, *Lunar Planet. Sci.* **14**, 704 (1983).
19. L. E. Nyquist, in *Proceedings of the 13th Lunar and Planetary Science Conference* (Pergamon, New York, 1982), p. A 785.
20. A. M. Vickery, *Lunar Planet. Sci.* **16**, 877 (1985).
21. P. N. Schultz and D. E. Gault, *ibid.*, p. 740.
22. H. A. Zook *et al.*, *ibid.* **15**, 965 (1984); D. E. Gault and J. A. Wedekind, in *Proceedings of the Ninth Lunar and Planetary Science Conference* (Pergamon, New York, 1978), pp. 3843–3875.
23. S. L. Thompson, SAND 77-1339, Sandia National Labs, Albuquerque, NM (1979).
24. T. J. Ahrens and J. D. O'Keefe, *Impact and Explosion Cratering*, D. J. Roddy, R. O. Pepin, R. B. Merrill, Eds. (Pergamon, New York, 1977), pp. 639–656.
25. G. Neukum and D. U. Wise, *Science* **194**, 1381 (1976).
26. D. E. Gault, *Moon* **6**, 32 (1973).
27. G. R. Cowan and A. H. Holtzmann, *J. Appl. Phys.* **34**, 928 (1963); H. El-Sopky, in *Explosive Welding, Forming, and Compaction*, T. Z. Blazynski, Ed. (Applied Science Englewood, NJ, 1983), pp. 189–217; S. W. Kieffer, in *Impact and Explosion Cratering*, D. J. Roddy, R. O. Pepin, R. B. Merrill, Eds. (Pergamon, New York, 1977), pp. 251–770).
28. J. E. Schouten, *Nuclear Geoplosics Sourcebook* (Report DNA6501H-4-2, Defense Nuclear Agency, Washington, DC, 1979), vol. 4, part 2; H. Mirels, "Blowing model for turbulence boundary-layer dust ingestion" (SD-TR-85-97, Aerospace Corp., El Segundo, CA 1986).
29. H. F. Swift and B. C. Clark, *Lunar Planet. Sci.* **14**, 765 (1983).
30. A. Henderson-Sellers, A. Benlow, A. J. Meadows, *Q. J. R. Astron. Soc.* **21**, 74 (1980).
31. Research supported under NASA grant NSG 7129. We appreciate the assistance of M. Lainhart with the calculations. We are grateful for the helpful comments proffered by G. Wetherill, D. Stevenson, D. Anderson, J. Melosh, B. C. Clark, D. E. Gault, and M. Kovari. Contribution 4137, Division of Geological and Planetary Sciences, California Institute of Technology, Pasadena, CA 91125.

14 March 1986; accepted 11 August 1986

Structure-Activity Studies of Interleukin-2

F. E. COHEN,* P. A. KOSEN, I. D. KUNTZ, L. B. EPSTEIN, T. L. CIARDELLI, K. A. SMITH

The critical role of interleukin-2 (IL-2) in immune response heightens the need to know its structure in order to understand its activity. New computer-assisted predictive methods for the assignment of secondary structure together with a method to predict the tertiary structure of a protein from data on its primary sequence and secondary structure were applied to IL-2. This method generated four topological families of structures, of which the most plausible is a right-handed fourfold α-helical bundle. Members of this family were shown to be compatible with existing structural data on disulfide bridges and monoclonal antibody binding for IL-2. Experimental estimates of secondary structure from circular dichroism and site-directed mutagenesis data support the model. A region likely to be important in IL-2 binding to its receptor was identified as residues Leu^{36}, Met^{38}, Leu^{40}, Phe^{42}, Phe^{44}, and Met^{46}.

THE IMMUNE SYSTEM IS A COMPLEX network of effector, helper, and suppressor cells that communicate and act through a myriad of macromolecules. This system is charged with surveillance and defense of the organism against intrinsic (oncologic) or extrinsic (microbiologic) insult. The T lymphocyte is an important component of host defenses. Elucidating the roles of T cells has been facilitated by the discovery of T-cell growth factors such as interleukin-2 (IL-2) (*1*). Interest in IL-2 has increased recently owing to reports of a possible role for this lymphokine in the treatment of solid tumors (*2*). Evidence already exists for a defect in IL-2 production by T lymphocytes of patients suffering from acquired immunodeficiency syndrome (*3*) and for a partial restoration of T-cell function by the addition of exogenous IL-2 in vitro (*4*).

Computer-assisted molecular modeling can be applied to macromolecules such as proteins. Methods for the prediction of secondary structure based on primary sequence have been developed by several investigators [for example, (*5*) and references therein]. Complementary methods for examining sequence-related hydropathy (*6*) allow one to predict interior and exterior regions of proteins as well as to suggest cytoplasmic, transmembrane, and potential binding sites for cell surface receptors (*7*). These methods are evolving rapidly as databases are strengthened with increased x-ray crystallographic data and the availability of recombinant DNA-derived protein sequences.

The primary structure of human and mouse IL-2 are available from complementary DNA (cDNA) sequences (*8*). A disulfide bridge links Cys^{58} to Cys^{105} (*9*). Secondary structure was assigned to the human sequence by use of the combinatorial pattern matching scheme of Cohen *et al.* (*5*). The four regions of α-helical structure recognized are listed in the legend to Fig. 1b. This assignment satisfies the sequential spacing of turns commonly observed in α-helical proteins, while simultaneously creating hydrophobic patches that facilitate helix-helix packing (see legend to Fig. 1b) (*10*). When the human and mouse sequences are compared, several features support our secondary structure assignment. A region containing 12 consecutive glutamine residues occurs sequentially adjacent to the amino terminus of mouse IL-2 helix A. Although it is difficult to appreciate the structural significance of the polyglutamine region, it is unlikely that this insertion is helical, and it cannot be a major functional feature. Further, substitutions occur more frequently in regions assigned as nonhelical (45% to 54%). Mutations that occur in regions assigned as helical are of a very conservative nature (for example, Ile^{24} → Leu^{24} and Ile^{28} → Met^{28} in the type III patch centered on residue 24).

Structural correlates for exon boundary locations have been proposed (*11*), including functional domains and small secondary structure assemblies. Frequently, exon boundaries occur in loop regions of proteins. This is true of the IL-2 exons 1–29, 30–49, 50–98, and 99–132 (*12*), with residues 30, 50, and 99 occurring at the boundaries of the predicted secondary structure.

Cohen *et al.* (*10*) developed a scheme for predicting the three-dimensional structure of α-helical proteins from the secondary structure. They used a combinatorial approach which generated millions of possible structures that satisfied the principles of pairwise helical packing. Tertiary structure restrictions were imposed to sort out unrealistic structures. Of 3×10^7 structures that were generated for myoglobin, only two satisfied the tertiary constraints (*10*). These two structures were similar and resembled

F. E. Cohen, Department of Pharmaceutical Chemistry, School of Pharmacy, and Department of Medicine, School of Medicine, University of California, San Francisco, CA 94143.
P. A. Kosen and I. D. Kuntz, Department of Pharmaceutical Chemistry, School of Pharmacy, University of California, San Francisco, CA 94143.
L. B. Epstein, Cancer Research Institute and Department of Pediatrics, University of California, San Francisco, CA 94143.
T. L. Ciardelli, Veterans Administration Hospital, White River Junction, VT 05001, and Department of Medicine, Dartmouth Medical School, Hanover, NH 03756.
K. A. Smith, Department of Medicine, Dartmouth Medical School, Hanover, NH 03756.

*To whom correspondence should be addressed.

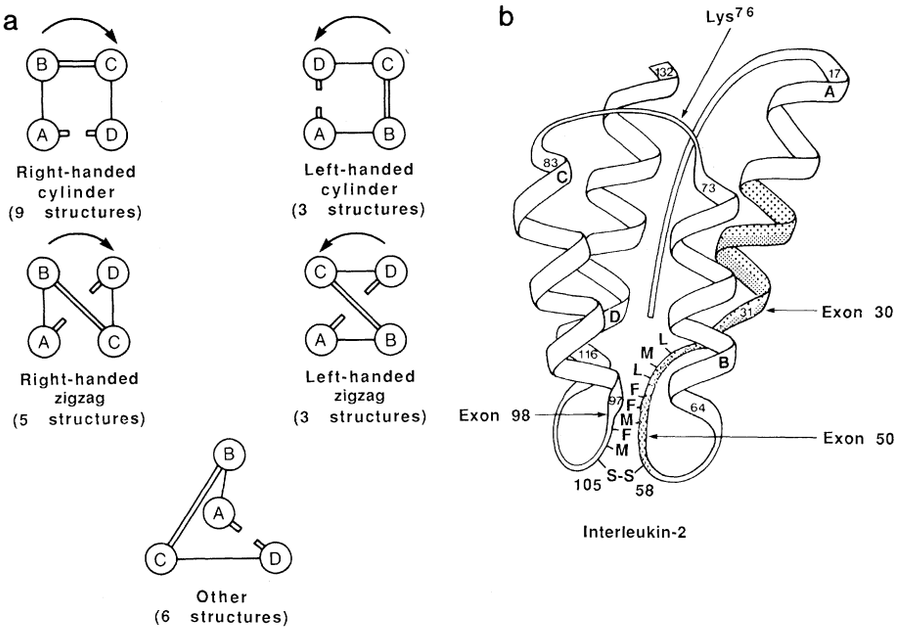

Fig. 1. (a) Schematic drawings of the helical topologies for the five families of predicted IL-2 structures. α-Helices are represented by circles and labeled sequentially A through D. They are shown end on. Connecting loops are shown as single or double lines. Double lines represent connections in front of the page, and single lines represent connections behind the page. Arrows highlight the sequential rotation of the helices. (b) Ribbon diagram of a member of the right-handed cylinder family of predicted IL-2 structures. Helical boundaries are located by a pattern-based turn scheme (*5*) with most turns located by the patterns pppp, pxppp, ppxpp, or pppxp, where p is a hydrophilic residue and x is any amino acid. Helices are segments bounded by turns with the patterns hqqhhqqh, hhqqhh, hqqqhhqqh, or hqqhhqqqh, where h is a hydrophobic residue and q tends to be hydrophilic. Helical boundary predictions have implied errors of ±3 residues. Helices are labeled A (17–31), B (64–73), C (83–97), and D (116–132), and the amino and carboxyl termini are numbered. Strong sites for helix-helix packing were determined by the method of Richmond and Richards (*11*). Interaction classes pertain to helix-helix docking angles II = −60° (residues 86 and 128) and III = 19° (residues 23, 24, 25, 69, 92, 93, 118, and 122). For further details, see Cohen *et al.* (*5*). The disulfide bridge between Cys^{58} and Cys^{105} is indicated. A collection of hydrophobic residues in the loop between helices A and B, which may be important in receptor binding, is marked. Exon boundaries are marked with arrows. The region of binding for monoclonal antibodies to 23–41 (dots), 27–41, (fine dots), and 42–60 (cross-hatch), which neutralize activity, are shown. Lys^{76}, a site of limited proteolysis, is also marked.

the crystallographic structure with a root-mean-square error of 4.5 Å. This procedure was subsequently applied to interferon-α (IFN-α) (*13*). When applied to IL-2, 3.9×10^4 structures were generated. Of these, 27 satisfy steric constraints while simultaneously maintaining the connectivity of the chain and permitting a disulfide bridge between residues Cys^{58} and Cys^{105}. The allowed structures can be placed into five structural categories: right-handed cylinder, right-handed zigzag, left-handed cylinder, left-handed zigzag, and others (Fig. 1a). Members of the last category of structure share the characteristic of a large surface-to-volume ratio, an unlikely feature for globular proteins. Weber and Salemme (*14*) observed only right-handed cylinders in a study of proteins known to form fourfold α-helical bundles. This family contains the largest number of permissible structures and is the most plausible assignment for the three-dimensional structure of IL-2 (Fig. 1b).

Although x-ray crystallography will be the final arbiter for the success of this IL-2 model, other physical studies can validate this prediction. The circular dichroism (CD) spectrum of human recombinant IL-2 was obtained (Fig. 2a) and fitted with several models to determine the percentage of α-helix and β-strand. The spectrum is characteristic of a protein with 49% to 65% α-helix and a smaller β-structure content. Our model contains 42% helix and no β-strands in the core structure. The percentage of helical structure within the core region is obviously sensitive to the exact assignment of the helical termini, which remains a difficult problem of secondary structure prediction and is often problematical even with the x-ray structure. Short α-helices or β-strands that are not part of the core structure could exist in the loop regions and contribute to the CD spectrum. The structural characteristics of the loop regions are not identified in our model.

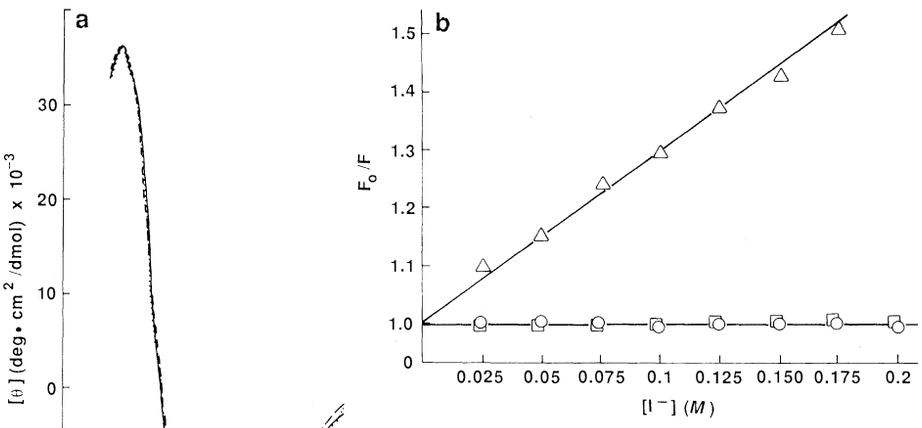

Fig. 2. (a) Far ultraviolet CD spectrum of recombinant human IL-2 (—) in 5 m*M* ammonium acetate (*p*H 5) at room temperature, recorded with a Jasco 500A spectropolarimeter. The spectrum is the average of three scans with protein concentrations of $3.4 \times 10^{-5}M$ and $2.2 \times 10^{-5}M$ determined with a molar extinction coefficient of $9.5 \times 10^3 M^{-1}$ cm^{-1} at 280 nm (*21*). [θ] is expressed as mean residue ellipticity. Also shown are the least-squares fits to the experimental spectrum by the procedures of Chang *et al.* (---) (*22*) and Provencher and Glockner (···) (*23*). Predicted fractions of secondary structure are $f_{helix} = 0.495$, $f_{sheet} = 0.235$, and $f_{remainder} = 0.27$, and $f_{helix} = 0.65$, $f_{sheet} = 0.35$, and $f_{remainder} = 0.0$, respectively. (b) Stern-Volmer plots of the I^- solute fluorescence quenching of single tryptophan-containing proteins: monellin (△), ribonuclease T1 (□), and recombinant IL-2 (○). Measurements were obtained at 29° ± 1°C in 0.1*M* phosphate buffer, *p*H 7.0 ($10^{-4}M$ $Na_2S_2O_3$), maintained at constant ionic strength by the addition of NaCl. Complete emission spectra (λ_{ex} = 295 nm) were recorded in triplicate at each concentration of I^-. Fluorescence values were determined at the wavelength of maximum emission for each protein (monellin, λ_{em} = 346 nm; ribonuclease T1, λ_{em} = 324 nm; recombinant IL-2, λ_{em} = 326 nm). No significant shifts were observed at higher concentrations of I^- (*24*).

Table 1. Structure-activity changes in IL-2. Summary of reported IL-2 structure modifications: (→) no significant change in biologic activity compared to recombinant IL-2 as determined and reported by the authors cited; (↓) an approximate decrease in activity of one order of magnitude; (↑) an approximate increase in activity of one order of magnitude; and (0) no biologic activity. ACM is the acetamidomethyl derivative of cysteine.

Structural change	Activity	Comment based on model	Reference
Modification			
Recombinant IL-2	→	Glycosylation not required for activity	(*25*)
N-Met IL-2	→	NH_2 terminus not important to activity	(*26*)
Des-Ala^1 IL-2	→	NH_2 terminus not important to activity	(*27*)
Mutation			
Cys^{125} → Ser	→↑	May enhance stability of helix D	(*4*)
Cys^{125} → Ala	↑	Enhances stability of helix D	(*28*)
Cys^{105} → Ala	↓	Precludes native disulfide	(*29*)
Cys^{105} → Ser	↓↓↓	Precludes native disulfide and places hydrophilic Ser near hydrophobic active loop	(*4*)
Cys^{58} → Ser	↓↓	Precludes native disulfide	(*4*)
Cys^{58} → Ala	↓↓	Precludes native disulfide	(*29*)
Met^{104} → Ala	→	Loop between C and D unimportant to activity	(*27*)
Phe$^{42\ \&\ 44}$ → Tyr	↓↓	Disruption of potential binding site	(*30*)
Phe$^{42\ \&\ 44}$ → Trp	↓↓↓	Disruption of potential binding site	(*30*)
Deletions			
Del 1–29	0	Loss of helix A	(*15*)
Del 30–49	0	Loss of binding site loop	(*15*)
Del 100–133	0	Loss of helix D	(*15*)
Del 114–133	0	Loss of helix D	(*30*)
Del 100–104, Cys^{125} ACM	↓↓	Possible to divide the chain creating two units, ABC and D, which can pack, preserving low level of activity	(*16*)
Del 100–104, Cys^{125}ACM, Trp^{121}*N*-formyl	0	Disruption of helix D packing site eliminates binding loop between helix B and C	(*16*)
Del 76-77, His^{79} → Asp	→	Unimportant to activity	(*30*)
Del Cys^{105}	↓	Loss of native disulfide	(*29*)
Del Cys^{58}	↓↓↓	Loss of native disulfide and deletion near active site	(*29*)
Del Cys^{125}	↓↓↓	Destabilizes helix-helix interaction for helix D	(*29*)
Del Phe^{125}	↓↓↓	Destabilizes helix-helix interaction for helix D	(*29*)
Del Gln^{126}	↓↓↓	Destabilizes helix-helix interaction for helix D	(*29*)

Further examination of the human and mouse sequences and the predicted tertiary structure showed a high proportion of conserved hydrophobic residues: Leu^{36}, Met^{39}, Leu^{40}, Phe^{42}, Phe^{44}, and Met^{46} in a peculiar region of the loop joining helices A and B. Since ligand-receptor binding is usually mediated by hydrophobic interactions, this region may be involved in IL-2 binding to its receptor. Monoclonal antibody data and site-directed mutagenesis can be used to test this prediction and simultaneously test the validity of the loop locations in the IL-2 model.

To identify the active region, we note that monoclonal antibodies characteristically bind to loops. The binding sites of most monoclonal antibodies to IL-2 have not been sufficiently determined to prove which residues are critical. However, antibodies exist to residues 1–12 and 71–87 (*15*) as well as to residues 23–41, 27–41, and 42–60. These antigenic sites correspond nicely to loops 1–19, 31–64, and 73–83. Neutralizing monoclonal antibodies are available that bind to some fraction of the residues in the local sequences 30–50 (*16*), 23–41 and 27–41 (*17*), and 42–60 (*15*). In a more direct approach, we have mutated Phe^{42} and Phe^{44} to Tyr and Trp with a stepwise decrease in activity. Further, proteolysis at Lys^{76} did not change activity (*18*); deletion of Lys^{76} and Asn^{77} did not change activity, although it did change the isoelectric point (*19*); and a semisynthetic hybrid missing residues 100–104 but containing the disulfide bridge Cys^{58} to Cys^{105} is active (*16*). These experiments also suggest that residues 76–77 and 100–104 are in loop regions with activity associated somewhere within residues 30–60. A complete list of mutagenesis experiments is included in Table 1.

Finally, site-directed mutagenesis can be used to explore helix-helix packing. Cys^{125} is part of a hydrophobic patch that includes Trp^{121}, Ile^{122}, Phe^{124}, and Ile^{128}. When Cys^{125} is mutated to Ser, activity is increased. This could be because of the enhanced stability given to the helix interaction site by eliminating a sulfur atom from a crowded interface or because Cys^{125} is chemically reactive. The former is supported by Cys^{125} → Ala which has increased activity over the Ser analog (*19*). These structural inferences will require experimental confirmation with CD. Fluorescence quenching experiments confirm that the environment of Trp^{121} is similar to the buried tryptophan in ribonuclease T1 but distinct from the exposed tryptophan in monellin (Fig. 2b).

Given the similarity in the predicted structure of the lymphokines IFN-α and IL-2, we began a preliminary search for other possible members of this structural family. Interleukin-3, IFN-β (which is homologous to IFN-α), and human growth hormone appear to be likely candidates. The sequences of IL-1α and IL-1β cannot readily be fitted into similar helical models and probably are not members of this group. Hydrophobic sequences in a region structurally analogous to the putative active loop of IL-2 are seen in IFN-α (Leu^{26}, Cys^{29}, Leu^{30}, Phe^{36}, and Phe^{38}) and in IFN-γ (Leu^{31}, Phe^{32}, Ile^{35}, Trp^{39}, Ile^{47}, and Met^{48}). Experiments by Alton *et al.* (*20*) on IFN-γ suggest that these residues may be important to activity since Trp^{39} → Phe causes a 90% decrease in activity and Met^{48} → Thr causes a 95% decrease in activity.

The major value of our calculations is their ability to generate testable models. To the extent that our model for the three-dimensional structure of IL-2 leads to experiments that clarify the function of IL-2 and aids in the design of analogs, the theoretical modeling process is valuable even if the details of the prediction fail.

Note added in proof. Zav'yalov and Denesyvk (*20a*) have proposed a five-helix bundle model for IL-2. We conclude that this model is incorrect because the distance between Cys^{58} and Cys^{105} would prevent the formation of the native disulfide bridge between these two residues.

REFERENCES AND NOTES

1. D. A. Morgan, F. W. Ruscetti, R. Gallo, *Science* **193**, 1007 (1976); S. Gillis and K. A. Smith, *Nature (London)* **268**, 154 (1977).
2. S. A. Rosenberg *et al.*, *N. Engl. J. Med.* **313**, 1485 (1985).
3. C. H. Kirkpatrick *et al.*, *J. Clin. Immunol.* **5**, 31 (1985); N. Ciobanu *et al.*, *ibid.* **3**, 332 (1983).
4. E. C. Ebert *et al.*, *Clin. Res.* **31**, 311A (1983); J. D. Lifson *et al.*, *Lancet* **1984-I**, 698 (1984).
5. F. E. Cohen *et al.*, *Biochemistry* **22**, 4894 (1983); *ibid.* **25**, 266 (1986).
6. J. Kyte and R. F. Doolittle, *J. Mol. Biol.* **157**, 105 (1982); T. P. Hopp and K. R. Woods, *Proc. Natl. Acad. Sci. U.S.A.* **78**, 3824 (1981).
7. W. J. Leonard *et al.*, *Nature (London)* **311**, 626 (1984); T. Nikaido *et al.*, *ibid.*, p. 631.
8. T. Taniguchi *et al.*, *ibid.* **302**, 305 (1983); N. Kashima *et al.*, *ibid.* **313**, 402 (1985).
9. A. Wang *et al.*, *Science* **224**, 1431 (1984).
10. F. E. Cohen, T. J. Richmond, F. M. Richards, *J. Mol. Biol.* **132**, 275 (1979); F. E. Cohen and M. J. E. Sternberg, *ibid.* **137**, 9 (1980).
11. W. A. Gilbert, *Nature (London)* **271**, 501 (1978); C. C. F. Blake, *ibid.* **273**, 267 (1978).
12. W. Degrave *et al.*, *EMBO J.* **12**, 2349 (1983).
13. M. J. E. Sternberg and F. E. Cohen, *Int. J. Biol. Macromol.* **4**, 137 (1982).
14. P. C. Weber and F. R. Salemme, *Nature (London)* **287**, 82 (1980).
15. R. Chizzonite *et al.*, *J. Cell. Biochem. Suppl.* **10A**, 73 (1986).
16. T. L. Ciardelli *et al.*, in *Peptides: Structure and Function*, C. M. Deber *et al.*, Eds. (Pierce Chemical, Rockford, IL, 1985), pp. 75–78.
17. J. Jenson, W. Danho, W. H. Tsien, M. Gately, *J. Cell. Biochem. Suppl.* **10A**, 76 (1986).
18. J. Browing and R. Mattaliano, *ibid.*, p. 73.
19. R. Gadski and T. Ciardelli, personal communication.
20. K. Alton *et al.*, in *The Biology of the Interferon System, 1983*, E. DeMaeyer and H. Schallekens, Eds. (Elsevier, Amsterdam, 1983), pp. 119–128.
20a. V. P. Zav'yalov and A. I. Denesyvk, *Immunol. Lett.* **10**, 71 (1985).
21. K. Kato *et al.*, *Biochem. Biophys. Res. Commun.* **130**, 692 (1985).
22. C. T. Chang, C. S. C. Wu, J. T. Yang, *Anal. Biochem.* **91**, 13 (1978).
23. S. W. Provencher and J. Glockner, *Biochemistry* **20**, 33 (1981).
24. S. S. Lehrer and P. C. Leavis, *Methods Enzymol.* **49**, 222 (1978).
25. K. Nauro *et al.*, *Biochem. Biophys. Res. Commun.* **128**, 257 (1985).
26. T. Yamada *et al.*, *ibid.* **135**, 837 (1986).
27. P. Ralph *et al.*, *J. Cell. Biochem.* **10A**, 71 (1986).
28. Amgen Technical Bulletin, 1985.
29. S. M. Liang, D. R. Thatcher, C. M. Liang, B. Allet, *J. Biol. Chem.* **261**, 334 (1986).
30. L. Butler *et al.*, *Immune Regulation by Characterized Polypeptides* (Liss, New York, in press).
31. Supported by grants GM34197 (to I.D.K.), NIH grants CA27903 and MOJ JD17001 (to L.B.E.), NIH grant ROA-ICA17643-11 (to K.A.S.), and grant VA00240324 and ACS grant IN157A (to T.L.C.). We thank J. T. Yang for the use of the spectropolarimeter and H. M. Martinez for the CD analysis programs.

14 May 1986; accepted 11 August 1986

Nerve Growth Factor Gene Expression in the Developing Rat Brain

THOMAS H. LARGE, SARAH C. BODARY, DENNIS O. CLEGG, GISELA WESKAMP, UWE OTTEN, LOUIS F. REICHARDT*

The regulation of nerve growth factor (NGF) protein and NGF messenger RNA (mRNA) in the developing rat brain has been studied to assess the hypothesis that NGF supports the differentiation of cholinergic neurons in the basal forebrain. In the adult, the major targets of these neurons, the hippocampus and neocortex, contain the highest concentrations of NGF mRNA, but comparatively low ratios of NGF protein to its mRNA. In contrast, a high concentration of NGF protein and a low concentration of NGF mRNA were seen in the basal forebrain, consistent with retrograde transport of NGF protein into this region from the neocortex and hippocampus. In these two target regions NGF and NGF mRNA were barely detectable at birth, their concentrations increased to a peak at day 21, and then NGF mRNA, but not NGF protein, declined threefold by day 35. NGF accumulation in the basal forebrain paralleled that in the target regions and preceded an increase in choline acetyltransferase, suggesting that the differentiation of cholinergic projection neurons is indeed regulated by retrogradely transported NGF. In addition, high ratios of NGF protein to NGF mRNA, comparable to that in the basal forebrain, were seen in the olfactory bulb and cerebellum, suggesting that NGF may be transported into these regions by unidentified neurons.

THE RELEASE OF DIFFUSIBLE TROPHIC factors by nerve cells and their targets has been thought to play a major role in the development and maintenance of connections in the nervous system (*1*). Although a number of putative trophic factors have been identified, only nerve growth factor (NGF) has been shown to be essential for neuronal survival in vivo, where it is required for the development of sympathetic and sensory neurons in the peripheral nervous system (*2*). Neurons in the central nervous system (CNS) may also depend on NGF during development since recent work has shown that the rat brain contains NGF (*3*), NGF messenger RNA (mRNA) (*3, 4*), NGF receptors (*5*), and NGF-responsive neurons (*6, 7*). Several lines of evidence suggest that one function of NGF in the CNS is to regulate the differentiation of the cholinergic projection neurons found within various nuclei of the basal forebrain. The hippocampus and neocortex, two regions innervated by these neurons (*8*), contain the highest levels of NGF protein and NGF mRNA found in the brain (*3, 4*). [^{125}I]-labeled NGF injected into cortical and hippocampal regions is transported retrogradely to the nucleus basalis (*9*) and the medial septum–diagonal band region (*10*), respectively. In neonatal rats, intraventricular injections of NGF increase choline acetyltransferase (ChAT) activity, the enzyme responsible for acetylcholine synthesis, in the basal forebrain (*11*). If NGF regulates cholinergic differentiation, then the target regions should be capable of supplying NGF to cholinergic fibers during the period of innervation. Our results show that the developmental increase in NGF content of the basal forebrain parallels that of the neocortex and hippocampus and precedes an increase of similar magnitude in ChAT activity, consistent with regulation of cholinergic differentiation by target-derived NGF.

NGF mRNA was measured in five brain regions of adult Sprague-Dawley rats by blotting polyadenylated [poly(A)$^+$] RNA onto nitrocellulose paper and hybridizing with a single-stranded NGF complementary DNA (cDNA) probe (*12*). NGF protein was measured by a two-site enzyme-linked immunosorbant assay (ELISA) with goat polyclonal and monoclonal antibodies to β-NGF (*13*). The hippocampus and neocortex contained relatively high amounts of both NGF and NGF mRNA (Table 1), in agreement with previous reports (*3, 4*). Although there also were large amounts of NGF in the basal forebrain, there was five times less NGF mRNA than in target regions. This is consistent with retrograde transport of NGF from the neocortex and hippocampus to the basal forebrain by cholinergic projection neurons (*9, 10*).

The hypothesis that NGF in the neocortex and hippocampus could provide trophic support for developing basal forebrain neurons was tested by comparing the increase in NGF content and ChAT activity of these regions during postnatal development. Because the neocortex and hippocampus con-

T. H. Large, S. C. Bodary, D. O. Clegg, L. F. Reichardt, Department of Physiology and Howard Hughes Medical Institute, University of California School of Medicine, San Francisco, CA 94143.
G. Weskamp and U. Otten, Department of Pharmacology, Biocentre of the University, Basel, Switzerland.

*To whom correspondence should be addressed.